Summer 8-15-2018

Assessment and Diagnosis of Human Ovarian and Colorectal Cancer using Optical and Photoacoustic Imaging

Sreyankar Nandy
Washington University in St. Louis

Recommended Citation

Nandy, Sreyankar, "Assessment and Diagnosis of Human Ovarian and Colorectal Cancer using Optical and Photoacoustic Imaging" (2018). *Engineering and Applied Science Theses & Dissertations*. 375.
https://openscholarship.wustl.edu/eng_etds/375

WASHINGTON UNIVERSITY IN ST. LOUIS

School of Engineering and Applied Science
Department of Biomedical Engineering

Dissertation Examination Committee:
Quing Zhu, Chair
Mark A. Anastasio
Matthew Lew
Yuan Chuan Tai
Lan Yang

Assessment and Diagnosis of Human Ovarian and Colorectal Cancer using Optical and Photoacoustic Imaging

by
Sreyankar Nandy

A dissertation presented to
The Graduate School
of Washington University in
partial fulfillment of the
requirements for the degree
of Doctor of Philosophy

August 2018
St. Louis, Missouri

Table of Contents

List of Figures

Acknowledgments

I would like to express my sincere gratitude and appreciation to my thesis advisor and dissertation committee chair Prof. Quing Zhu, who has guided me throughout my Ph.D. studies with patience and sincerity, motivating me with her positive attitude, unselfish rigor and taught me to approach important clinical and scientific problems with dedication and integrity.

I am especially thankful to my colleagues from the Optical and Ultrasound Imaging laboratory at University of Connecticut and Washington University in St. Louis, including Dr. Tianheng Wang, Dr. Patrick Kumavor, Dr. Hassan Salehi, Dr. Hai Li, Dr. Mohsen Erfanzadeh, Dr. Bin Rao, Atahar Mostafa, Yifeng Zheng, Xiandong Leng, Eghbal Amidi and Guang Yang. The current work would not have been completed successfully without their contributions.

I would like to thank my committee members Drs Mark Anastasio, Yuan Chuan Tai, Matthew Lew and Lan Yang for their valuable suggestions and constant support.

Finally, I owe the successful completion of my dissertation to my family, including my parents and my wife, who have supported me throughout my Ph.D. journey with their love, encouragement and unconditional support.

Sreyankar Nandy

Washington University in St. Louis

August 2018

Dedicated to my parents and my wife.

ABSTRACT OF THE DISSERTATION

Assessment and Diagnosis of Human Ovarian and Colorectal Cancer using Optical and Photoacoustic Imaging

by

Sreyankar Nandy

Doctor of Philosophy in Biomedical Engineering

Washington University in St. Louis, 2018

Professor Quing Zhu, Advisor and Chair

Optical imaging modalities have the advantage of high resolution, label free, rapid, low cost imaging for both *in vivo* and *ex vivo* diagnosis of biological tissues. Optical scattering, which is the main contrast of optical coherence tomography (OCT), is related to elastic scattering components, mainly stromal collagen. Tissue elasticity has recently emerged as an important diagnostic parameter associated with tumor development and progression and is also related to the distribution of structural components such as tissue collagen. We have used an optical coherence tomography elastography (OCTE) system for characterizing the differences in the micro-mechanical properties of benign and malignant human ovarian tissue and correlated with the corresponding tissue collagen content (chapter 1). Additionally, spatial heterogeneity has also been associated with diagnosis of normal and malignant tissue. Automated image recognition and analysis can be a useful tool for overcoming the limitations of observer-dependent visual identification and discrimination of normal and malignant features of tissue. We developed a high-resolution full field optical coherence tomography (FFOCT) system for classification of the morphological changes associated with the progression of human ovarian cancer (chapter 2). Optical absorption reveals contrast related to the tumor microvasculature and tumor angiogenesis.

Absorption information from two or more wavelengths can provide functional information such as total blood hemoglobin as well as blood oxygen saturation, which is related to tumor angiogenesis and tumor hypoxia. Spatial frequency domain imaging (SFDI) is a powerful wide field, label free imaging modality sensitive to both optical absorption as well as scattering, which can be used together for complete assessment of normal and diseased tissues. SFDI was used for multispectral, *ex vivo* assessment of different types of human ovarian and colon tissue with considerable accuracy (chapter 3). For *in vivo* optical diagnosis of human ovarian cancer, the main limitation has been the shallow depth of penetration due to intense scattering from the biological tissue, which requires direct contact with the tissue surface and requires invasive procedures. Photoacoustic tomography combined with ultrasound (PAT/US) was used to overcome this limitation by using NIR light combined with diagnostic frequency ultrasound to achieve a depth of up to 5 cm with considerable resolution and correspondingly provide functional information related to tumor angiogenesis and oxygen saturation (chapter 4).

Chapter 1 Introduction

1.1 Motivation

The mortality rate for ovarian cancer is the highest among all the gynecological cancers [1,2]. 5-year survival rate is usually very high (70-90%) if detected in early stages such as Stage I and Stage II, yet, due to lack of currently available effective screening and early diagnostic techniques, most ovarian cancers are detected only at later stages (Stage III and IV), where the 5-year survival rate can be as low as 17%. Prophylactic oophorectomy (PO) remains the standard preventive measure, which has been shown to reduce the risk of ovarian cancer by 50% [3,4]. However, for premenopausal women undergoing PO, there is an increased risk of developing breast cancer as well as potentially life-threatening complications arising from premature menopause [5].

The imaging modalities currently used are expensive and lack the efficacy to detect early stage ovarian cancer. Available techniques include serum marker CA125 (sensitivity <50%) screening, transvaginal ultrasound (US) (3.1% PPV), and pelvic exams (sensitivity around 30% [6]) . Imaging technologies such as CT and MRI are costly and may not provide very high yield [7]. Positron emission tomography (PET), although successful in assessment and diagnosis of tumor metastasis, but needs specific tracers (18F-FDG) and is limited in detection of early stage cancers [8]. For *ex vivo* assessment, histology remains the gold standard, however it also requires staining and considerable wait time for diagnosis. Therefore, there is an unmet need for developing sensitive tools for early detection and diagnosis of ovarian cancer, to alleviate the risk associated with nd rectum is the second is the second most common cancer type globally and the 4th leading cause of cancer deaths. In the US, there are approximately 40,000 cases of rectal cancer diagnosed annually

[9]. Current screening methods include proctectomy (surgical removal of the rectum) and preoperative radiation and postoperative chemotherapy, depending on the stage of disease. It is critical to be able to determine the depth of tumor invasion and identify any potential metastatic lymph nodes in order to determine the most appropriate treatment regimen for each tumor. However, current imaging tools like MRI and endoscopy cannot reliably differentiate islands of surviving tumor and their micro-vessel network from the scar produced by dying cancer. Other imaging modalities**,** endoscopic ultrasound (EUS), CT, PET have a limited role in evaluating tumor stage [10]. Surgeons today can only identify complete responders after surgery. Therefore, there is critical need for new rectal imaging modalities that can accurately identify complete responders prior to surgical excision.

1.2 Optical and Photoacoustic Imaging

Optical imaging has emerged as an important biomedical imaging modality that can provide high resolution, label free, functional and structural information of biological tissues without using ionizing radiation.

Optical coherence tomography (OCT), which measures back-scattered light from biological tissues, can achieve sub-cellular resolution with a depth of penetration of couple of mm [11]. OCT has been used for numerous diagnostic applications such as ophthalmology, dermatology, breast cancer, colon cancer, dentistry, gastrointestinology etc. [12, 13]. OCTE is an extension of conventional OCT, which can be used to map the microscopic changes in the tissue elastic properties. OCTE can be either static, where the strain can be qualitatively evaluated from the displacement of the tissue under excitation, or dynamic, where a quantitative measurement of the shear modulus of the tissue can be performed by detecting the velocity of high frequency ultrasonic shear waves [14].

Spatial frequency domain imaging (SFDI) is based on the principle of diffuse optical propagation of light in the spatial frequency domain, which is sensitive to both light absorption and scattering [15]. Sinusoidal patterns of spatial frequencies are projected on the tissue surface with different phase, and from the diffuse reflected light, the optical chromophore information such as blood hemoglobin, oxygen saturation, water, lipid etc. can be obtained with accuracy over a large field of view. The method is low cost, rapid, label free and has found numerous application in dermatology, breast cancer, ovarian cancer imaging as well as monitoring cortical hemodynamics, drug delivery, burn injury, Alzheimer’s disease detection [16-18].

Photoacoustic tomography (PAT) is a combination of optical and ultrasound modalities. In PAT, a short-pulsed laser illuminates the biological tissue [19, 20]. The tissue undergoes thermal expansion and as a result generates acoustic or photoacoustic waves, which is then detected by ultrasound transducers and subsequently used to map the absorption distribution inside the tissue. In the NIR wavelength (600-900 nm), blood oxy and de-oxy hemoglobin are the main optical absorbers, and the photoacoustic imaging can provide precise functional information related to angiogenesis and blood oxygen saturation, which are important prognosticators of tumor growth and metabolism. PAT has shown great potential in recent years for diagnosis of breast, skin, brain and ovarian tissue diagnosis [21, 22].

1.3 Organization of the Dissertation

The current dissertation is organized into 5 chapters.

Chapter 1 provides the background and motivation of the current research, as well as introducing different optical and photoacoustic imaging modalities. **Chapter 2** describes the application of

OCTE for characterizing the micro-mechanical properties of normal and malignant human ovarian tissue. In **chapter 3**, application of FFOCT system for assessing the morphological differences between different ovarian tissue groups is described. **Chapter 4** describes the application of SFDI for multispectral discrimination of different groups of human ovary and colon tissue. The application of PAT/US for *in vivo* imaging of human ovarian cancer patients and the corresponding results are described in **chapter 5**. Finally, the summary of the current work and future developments are discussed in **chapter 6**.

References

[1] American Cancer Society, "Cancer Facts & Figures 2017," American Cancer Society (2017).

[2] Hoskins.W.J., "Prospective on ovarian cancer: why prevent ?," J Cell Biochem Suppl 23,189-199 (1995).

[3] U.S. Preventive Services Task Force. "Screening for Ovarian Cancer: Recommendation Statement," (2004).

[4] Maehle L. et al, "High risk for ovarian cancer in a prospective series is restricted to BRCA1/2 mutation carriers," Clin Cancer Res. 2008 Nov 15;14(22):7569-73.

[5] Kauff N.D., Domchek S.M., Friebel T.M. et al.," Risk-reducing salpingo-oophorectomy for the prevention of BRCA1- and BRCA2-associated breast and gynecologic cancer: a multicenter, prospective study", J Clin Oncol. 2008 Mar 10; 26(8):1331-7.

[6] Nossov V., Amneus M., Su F., Lang J., Janco J.M., Reddy S.T. and Farias-Eisner R., "The early detection of ovarian cancer: from traditional methods to proteomics. Can we really do better than serum CA-125?" Am J Obstet Gynecol 199(3), 215-223 (2008).

[7] Tammela J. and Lele S., "New modalities in detection of recurrent ovarian cancer," Curr Opin Obstet Gynecol 16(1), 5-9 (2004).

[8] R. Bristow, R. Giuntoli., HK. Pannu et al. “Combined PET/CT for detecting recurrent ovarian cancer limited to retroperitoneal lymph nodes,” Gynecologic Oncology, 99 (2005) 294-300.

[9] American Cancer Society. Colorectal Cancer Facts & Figures 2017-2019. 2017.

[10] Moreno, C.C., P.S. Sullivan, and P.K. Mittal, MRI Evaluation of Rectal Cancer: Staging and Restaging. Curr Probl Diagn Radiol, 2016.

[11] Fujimoto J. G., Pitris C., Boppart B. A., Brezinski and M. E., “Optical coherence tomography: an emerging technology for biomedical imaging and optical biopsy,” Neoplasia 2(1-2), 9-25 (2000).

[12] Vakoc B. J., Fukumura D., Jain R. K., and Bouma B. E., “Cancer imaging by optical coherence tomography: preclinical progress and clinical potential,” Nat. Rev. Cancer 12(5), 363-368 (2012).

[13] Karanasos A., Ligthart J., Witberg K., van Soest G., Bruining N., and Regar E., “Optical coherence tomography: potential clinical applications,” Curr. Cardiovasc. Imaging Rep. 5(4), 206-220 (2012).

[14] Larin KV, Sampson DD. Optical coherence elastography – OCT at work in tissue biomechanics [Invited]. Biomed Opt Express. 8(2):1172-1202, (2017).

[15] Cuccia, David J. et al. “Quantitation and Mapping of Tissue Optical Properties Using Modulated Imaging.” J Biomed Opt.14.2 (2009).

[16] Chen Xinlin et al, “In vivo real-time imaging of cutaneous hemoglobin concentration, oxygen saturation, scattering properties, melanin content, and epidermal thickness with visible spatially modulated light,” Biomed Opt Express, 8(12), (5468), (2017).

[17] Lin, A. J. et al, “Spatial Frequency Domain Imaging of Intrinsic Optical Property Contrast in a Mouse Model of Alzheimer’s Disease.” Annals of Biomedical Engineering, 39(4), 1349–1357 (2011).

[18] Nandy S, Mostafa A, Kumavor PD, Sanders M, Brewer M, Zhu Q, “Characterizing optical properties and spatial heterogeneity of human ovarian tissue using spatial frequency domain imaging.” J. Biomed. Opt; 21(10), (2016).

[19] Wang L. V. and Hu S., “Photoacoustic tomography: in vivo imaging from organelles to organs,” Science 335, 1458-1462 (2012).

[20] Xu M.H. and Wang L.H.V., “Photoacoustic imaging in biomedicine,” Rev. Sci. Instrum. 77(4), 041101 (2006).

[21] Aguirre A. et al, "Coregistered three-dimensional ultrasound and photoacoustic imaging system for ovarian tissue characterization,” J. Biomed. Opt; 14(5), 054014 (2009).

[22] Heijblom M. et al. “The State of the Art in Breast Imaging Using the Twente Photoacoustic Mammoscope: Results from 31 Measurements on Malignancies.” European Radiology 26.11 3874–3887, (2016).

Chapter 2 Characterizing the stiffness difference between benign and malignant human ovarian tissue using optical coherence tomography based elastography (OCTE) system

2.1 Background

About 95% of all ovarian cancers originate from the epithelial layer cells on the outer surface of the ovarian tissue, which makes the malignant ovarian tissue surface much softer compared to the normal tissue. Thus, the relative difference in stiffness is expected to provide the mechanical contrast between healthy and malignant ovarian tissues for diagnosis [1]. Collagen in the extracellular matrix is the main structural protein component of the ovarian tissue [2]. Previous optical coherence tomography (OCT) studies from have shown that the amount of collagen is an accurate marker for ovarian cancer detection [3]. Optical coherence elastography (OCE) is an extension of conventional OCT, which can measure the micro-mechanical properties of biological tissues [4, 5]. The main principal of OCE is to apply a load to the biological tissue, either through acoustic radiation force (ARF) and measure the quantitative elastic modulus [6, 7], or measure displacement and strain, which can then be used to characterize the tissue elasticity [8, 9]. We report in this study, to the best of our knowledge, the first exploratory study showing the feasibility of a catheter-based swept source OCT system for calculating the strain inside human ovarian tissue as well as measure the correlation between the measured strain with the collagen content of the ovarian tissue. The work in this chapter has been published in Biomedical Optics Express [10].

2.2 Materials and Methods

2.2.1 OCT Elastography system

Details of the phase stabilized swept source OCE system is shown in figure 2.1, which is based on a 1310 nm swept source (HSL-2000, Santec Corp., Japan) with a bandwidth of 110 nm and scan rate of 20 kHz. The 10 mW output power from the swept source was evenly split into reference and sample arms by a 2 × 2 coupler. The backscattered light was collected by a side view ball lens catheter (WT&T Inc., Canada, diameter 0.5 mm) and recombined with the reference light at the second 2 × 2 coupler. The interference signal was detected by a balanced detector (Thorlabs PDB120C) and acquired by a 50 MHz digitizer (Cs8325, Gage Applied) after a 20 MHz anti-alias filter. The axial resolution of the system in air was 12µm at a distance of 1mm from the focus. The phase jitter of the swept source was removed by using a narrow band fiber bragg grating (OE Land, $\lambda o = 1310$ nm, $\Delta\lambda = 0.096$ nm, reflectivity> 99%) as the trigger for A-scan acquisition. To account for the optical power variation during the A-line scans, a wavelength dependent amplitude correction was applied to the raw data and the scaled measurement data was interpolated to a uniform grid in the k-space before Fourier transform. The phase stability of the swept source OCT system was measured to be ~7 mrads, which correspond to a displacement sensitivity of 1.4 nm in air.

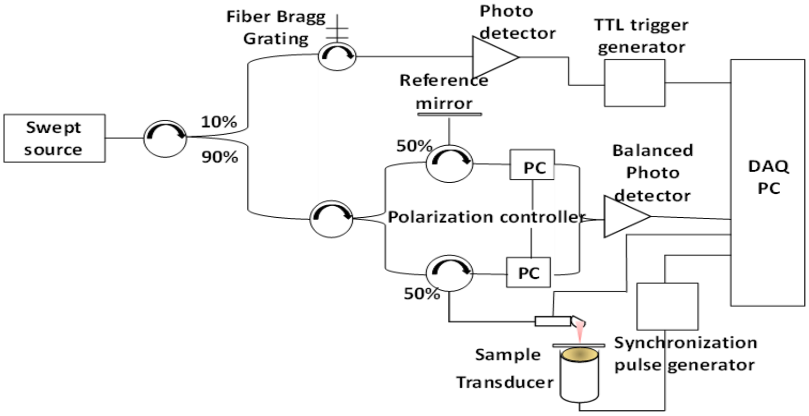

Figure. 2.1. OCTE system configuration. Swept Source OCTE system.

2.2.2 Calculation of Displacement and Strain

Ovarian tissue samples were placed between an unfocused transducer (Krautkramer Alpha) and a cover slide of thickness 140 μm. This transducer has a frequency response from several Hz to 300 KHz. A square wave (500 Hz, 50% duty cycle), generated by a function generator synchronized with the data acquisition system was used to periodically compress the sample in the axial direction between the transducer surface and the glass cover slide. For most of the imaging purposes, the catheter probe was kept fixed (no axial scanning) and M-mode images were acquired. 600 A-lines were averaged for each M-mode image to reduce the effect of any residual sample arm jitter and to improve the SNR of the measured displacement. The acquisition time for each M-mode image was 30 ms. The displacement amplitude and corresponding strain was calculated from 50~100 locations, at a separation of 5µm depending on the size of ovary sample. The overall acquisition time for each ovary sample was < 1 sec, which makes the system suitable for potential *in vivo* applications. An example of a normal and malignant ovarian tissue is shown in Fig. 2.2. The representative B-scan images of the normal and malignant samples are shown in Fig. 2.2(a) and Fig. 2.2(e). The white dashed rectangular area in the B-scan images represent the area from which M-mode images were acquired as shown in Fig. 2.2(b) and Fig. 2.2(f) respectively. The displacement at each location is measured from the phase difference between the pre-compression and post-compression A-lines. The strain inside the tissue can be estimated from the slope of the displacement curve. The average displacement was estimated for each sample and the corresponding average strain was calculated by linear least square fitting of the displacement curve, as shown in Fig. 2.2(d) and Fig. 2.2(h). Phase stability of an endoscopic swept source OCE system can be challenging due to the jitter induced by the trigger and slow linear/rotational scanning movement of the stepper motor [11]. Using the M mode detection scheme, a rapid estimation of overall tissue elasticity can be obtained [12, 13]. It should be noted though that the measured strain is dependent on the experimental conditions, and a strict quantification of the elasticity of the ovarian tissue can only be done by exact measurement of the Young’s modulus [14]. However, assuming a uniform distribution of stress throughout the sample, the displacement and strain can provide the corresponding relative mechanical contrast, comparable to the elastic moduli [15].

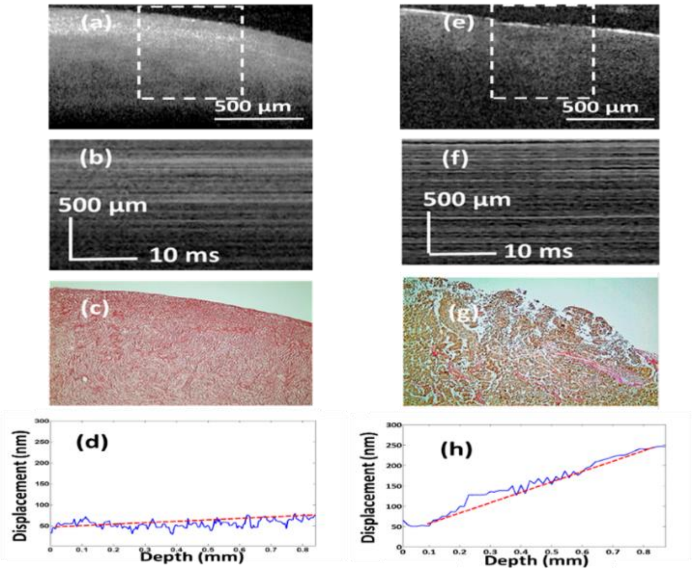

Figure. 2. 2 Examples of FFOCT images. Normal [(a) - (d)] and malignant [(e) - (h)] ovarian tissue. (a) and (e) OCT B-scan images, (b) and (f) M-mode images, (c) and (f) SR stains showing collagen distribution, (d) and (h) corresponding averaged displacement curves. Slope of the least square fitted red dashed lines in (d) and (h) represent the average strain.

2.2.3 Human ovary study

Ovary samples were obtained from patients undergoing PO at the University of Connecticut Health Center (UCHC). The patients were at risk for ovarian cancer or they had an ovarian mass suggestive of malignancy. This study was approved by the Institutional Review Boards (IRB) of UCHC, and informed consent was obtained from all patients. Ovaries were kept in 0.9% wt/vol NaCl solution and imaged within 24 hours after oophorectomy. After OCT imaging, the ovaries were fixed in 10% formalin solution and returned to the Pathology Department for histological processing.

2.2.4 Histology and Collagen Area Fraction

After the imaging, the ovary samples were cut in 5 mm blocks parallel to the imaging plane, dehydrated with graded alcohol, embedded in paraffin and sectioned to 7 μm thickness using a paraffin microtome. The slides that correspond to the imaged planes were identified, and stained using Hematoxylin and Eosin (H&E) for diagnosis. For quantification of the collagen content inside the tissue, adjacent cross-section (7 μm apart from H&E cross-section) was sliced and stained with Sirius Red, which specifically binds to tissue collagen [16]. The digital image of the surface histology covering about 1 mm depth was acquired using a bright field microscope, shown in Fig. 2(c) and Fig. 2(g). The amount of collagen was quantified using ImageJ software. The collagen area fraction (CAF) was measured as “stained collagen area/tissue area.”

2.3 Results and Discussions

A total of 27 ovaries from 16 patients (aged 39-76 years; mean, 57 years) were imaged using the OCE system. The ovarian tissues were diagnosed according to the histopathology as normal (n =

22), abnormal (n = 2), and malignant (n = 3). The H&E histology and Sirius Red stain of the normal ovarian samples exhibited homogeneous and compact collagen distribution. The group of ovaries with abnormal diagnosis consisted of surface endometriosis with trace amount of dense stroma, while the malignant ovarian tissue group consisted of serous carcinoma, severe necrosis and characterized by highly degenerated and scattered collagen distribution.

The displacement amplitude and corresponding strain rate was calculated from 50~100 locations, at a separation of 5µm depending on the size of ovary sample. The local strain rate was measured for a total of 1670 locations, including 1215 from normal, 175 from abnormal and 280 from malignant ovaries. The histograms of micro strain (με) rate of normal and malignant ovarian tissue groups are shown in Fig. 3(a). The average strain rate obtained for the normal tissue group was 23.05 με (± 10.74), while the average strain rate inside the abnormal and malignant group was 42.3 με (± 11.11) and 54.14 με (± 11.68), respectively. The ratio of the average strain rate of the malignant and normal tissue groups was 2.35, signifying much softer tissue structure in the malignant ovaries. The comparison between normal, abnormal and malignant groups by Student's t-test is shown in Fig. 3(b). The difference between the normal-malignant ($p < 0.001$) and normal-abnormal ($p < 0.001$) was found to be highly statistically significant. The comparison between the abnormal and malignant group, though significant, was much closer ($p = 0.047$). This can be attributed to the fact that the abnormal samples consisted of epithelial endometriosis, which may be associated with the development of cancer [17] and causes alterations in the connective tissue of the ovary. The receiver operating characteristic (ROC) curve which plots the true positive ratio (TPR) versus false positive ratio (FPR) between the normal and malignant groups is shown in Fig. 2.3(c). The area under the curve (AUC) is 0.902. Using 25 με as the threshold, a sensitivity of 93.2% and a specificity of 83% was achieved.

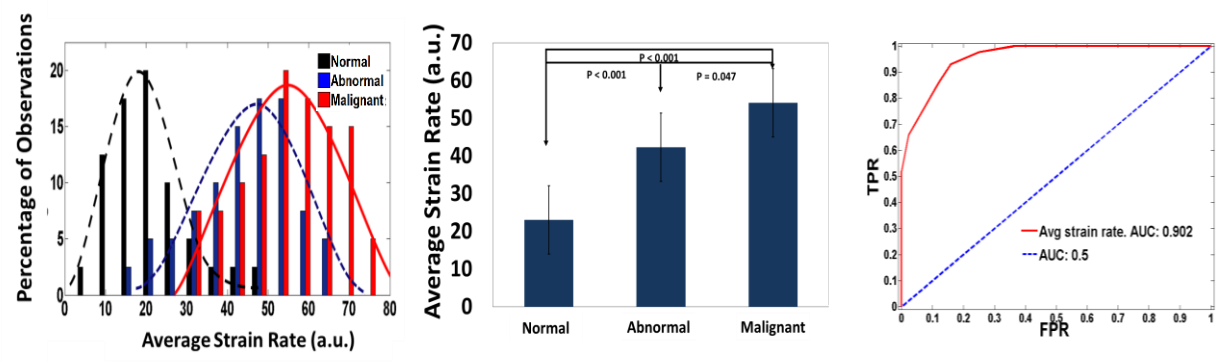

Figure. 2.3 Results from strain measurements. (a) Histograms of με obtained from normal, abnormal and malignant ovarian tissue groups, along with Gaussian distribution fits. (b) Statistics of normal, abnormal and malignant groups. (c) ROC curve of με.

Figure 2.4 (a) shows the histograms of CAFs obtained from normal, abnormal and malignant ovarian tissue groups. The average CAF of normal group was 47.4% (± 12.3%), while the average CAF of the abnormal and malignant group was 19.85% (± 7.25%) and 10.11% (± 3.22 %). The statistical significance between these groups is shown in Fig. 2.4(b). The ROC curve obtained from the CAF as shown in Fig. 2.4(c), to compare with the ROC curve obtained from strain measurements. A sensitivity of 95% and a specificity of 100% were obtained by using 22% CAF as optimum threshold. The AUC obtained from CAF is 0.988.

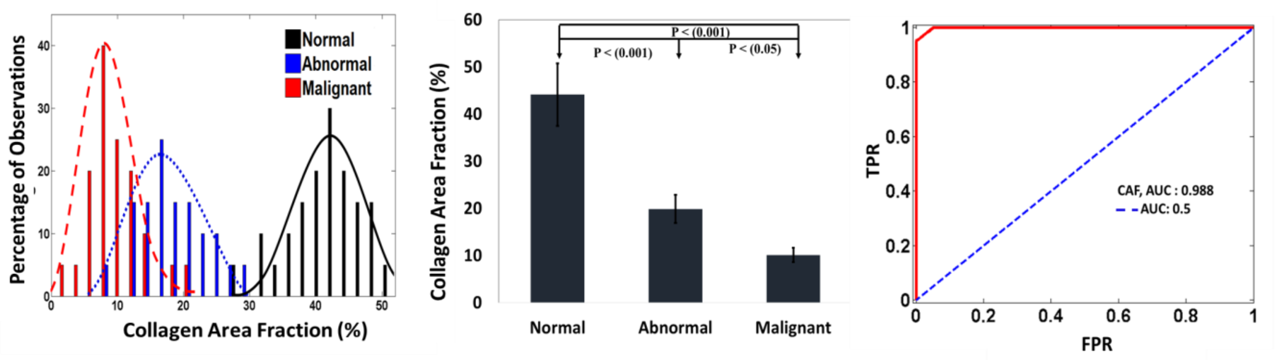

Figure. 2.4

Figure. 2.4 Results from CAF. (a) Histograms of CAF obtained from normal, abnormal and malignant ovarian tissue groups, along with Gaussian distribution fits. (b) Statistics of normal, abnormal and malignant groups. (c) ROC curve of CAF.

A linear regression analysis shown in Fig.2.5 demonstrates strong negative correlation (R =-0.75, p < 0.0001) between the collagen content inside the ovarian tissue and average strain rate. A highly mature, dense distribution of collagen fibers provides much higher stiffness to the normal ovarian tissue, whereas for endometriosis and development of epithelial ovarian cancer, the collagen structure gradually degenerates and in effect the ovarian tissue becomes much softer and deformable. The trace amount of elastin that might be present in the walls of the vessels would not be a major contributor to the overall elasticity of the ovarian tissue.

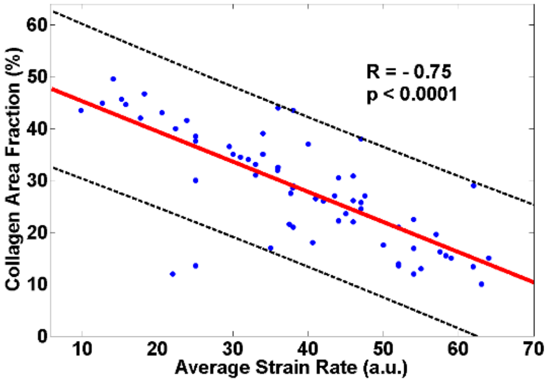

Figure. 2.5 Correlation between estimated strain rate and tissue collagen content. The black dashed lines show 95% prediction intervals.

2.4. Summary

In this study, 27 ovary samples obtained from 16 patients were studied *ex vivo* using the catheter-based phase stabilized swept source OCE system. Average displacement amplitude was estimated inside the tissue samples from the phase difference of the pre-compression and post-compression A-lines. The average strain rate was calculated by linear least square fitting of the displacement curve, under the assumption of uniform stress and mechanical equilibrium. A sensitivity of 93.2% and a specificity of 83% were achieved for the normal and malignant tissue groups using strain rate. The amount of collagen inside the tissue was quantified by Sirius Red staining and found to have a strong negative correlation with the average strain rate, indicating a softer and degenerated tissue structure in the malignant group as compared to the normal ovarian tissue. The initial results indicate that OCE can be a robust method for ovarian cancer detection and diagnosis and a potential guidance tool for surgeons during minimally invasive surgery.

References

[1] Xu, Wenwei et al. “Cell Stiffness Is a Biomarker of the Metastatic Potential of Ovarian Cancer Cells.” Ed. Surinder K. Batra. PLoS ONE 7.10 (2012).

[2] Lind A. K. et al, “Collagens in the human ovary and their changes in the perifollicular stroma during ovulation,” Acta Obstet Gynecol Scand; 85(12):1476-84 (2006).

[3] Wang T., Brewer M., Zhu Q., “An overview of optical coherence tomography for ovarian tissue imaging and characterization,” Wiley Interdiscip. Rev. Nanomed. Nanobiotechnol. 7(1):1-16 (2015).

[4] Schmitt J., “OCT elastography: imaging microscopic deformation and strain of tissue,” Opt. Express 3(6), 199–211 (1998).

[5] Wang R. K., Ma Z. H., Kirkpatrick S. J., “Tissue Doppler optical coherence elastography for real time strain rate and strain mapping of soft tissue,” Appl. Phys. Lett. 89(14), 144103 (2006).

[6] Qi W., Chen R., Chou L., Liu G., Zhang J., Zhou Q., Chen Z., “Phase-resolved acoustic radiation force optical coherence elastography,” J. Biomed. Opt. 17(11), 110505 (2012).

[7] Zhu J., Qu Y., Ma T., Li R., Du Y., Huang S., Shung K. K., Zhou Q., Chen Z., “Imaging and characterizing shear wave and shear modulus under orthogonal acoustic radiation force excitation using OCT Doppler variance method,” Opt. Lett. 40(9), 2099–2102 (2015).

[8] Wang R. K., Kirkpatrick S., Hinds M., “Phase-sensitive optical coherence elastography for mapping tissue microstrains in real time,” Appl. Phys. Lett. 90(16), 164105 (2007).

[9] Guan G., Li C., Ling Y., Yang Y., Vorstius J. B., Keatch R. P., Wang R. K., Huang Z., “Quantitative evaluation of degenerated tendon model using combined optical coherence elastography and acoustic radiation force method,” J. Biomed. Opt. 18(11), 111417 (2013).

[10] S. Nandy, H. S. Salehi, T. Wang, X. Wang, M. Sanders, A. Kueck, M. Brewer, and Q. Zhu, “Correlating optical coherence elastography based strain measurements with collagen content of the human ovarian tissue,” Biomed. Opt. Express 6(10), 3806–3811 (2015).

[11] Liu G., Tan O., Gao S. S., Pechauer A. D., Lee B., Lu C. D., Fujimoto J. G., Huang D., “Postprocessing algorithms to minimize fixed-pattern artifact and reduce trigger jitter in swept source optical coherence tomography,” Opt. Express 23(8), 9824–9834 (2015).

[12] Manapuram R. K., Aglyamov S. R., Monediado F. M., Mashiatulla M., Li J., Emelianov S. Y., Larin K. V., “In vivo estimation of elastic wave parameters using phase-stabilized swept source optical coherence elastography,” J. Biomed. Opt. 17(10), 100501 (2012).

[13] Kennedy K. M., McLaughlin R. A., Kennedy B. F., Tien A., Latham B., Saunders C. M., Sampson D. D., “Needle optical coherence elastography for the measurement of microscale mechanical contrast deep within human breast tissues,” J. Biomed. Opt. 18(12), 121510 (2013).

[14] Razani M., Mariampillai A., Sun C., Luk T. W. H., Yang V. X. D., Kolios M. C., “Feasibility of optical coherence elastography measurements of shear wave propagation in homogeneous tissue equivalent phantoms,” Biomed. Opt. Express 3(5), 972–980 (2012).

[15] Kirkpatrick S. J., Wang R. K., Duncan D. D., “OCT-based elastography for large and small deformations,” Opt. Express 14(24), 11585–11597 (2006).

[16] Malkusch W., Rehn B., Bruch J., “Advantages of Sirius Red staining for quantitative morphometric collagen measurements in lungs,” Exp. Lung Res. 21(1), 67–77 (1995).

[17] Dzatic-Smiljkovic O., Vasiljevic M., Djukic M., Vugdelic R., Vugdelic J., “Frequency of ovarian endometriosis in epithelial ovarian cancer patients,” Clin. Exp. Obstet. Gynecol. 38(4), 394–398 (2011).

Chapter 3 Analysis and Classification of High Resolution Images from Full Field Optical Coherence Tomography (FFOCT) System for Rapid, Label Free Diagnosis of Human Ovarian Tissue Samples

3.1 Background

Optical coherence tomography (OCT) has proved to be useful for *ex vivo* and *in vivo* detection of ovarian cancer, mainly because it can detect the microscopic changes in the stromal collagen distribution which results in alteration of tissue scattering and elasticity. In general, point detectors or line detectors are required for generating OCT images. However, this requires extensive scanning, and is limited by the field of view. Full field optical coherence tomography (FFOCT) which is an extension of conventional OCT, can acquire high resolution en face interferometric images with an area detector e.g. a CMOS or CCD camera. The axial resolution is determined by the bandwidth of the light source, which is generally a very broadband low-cost halogen lamp. This can provide a very high axial resolution of 1-2 μm, compared to the conventional SLD based sources [1, 2]. The transverse resolution of the system can be controlled by the numerical aperture of the microscope objectives and the source wavelength. FFOCT provide greater contrast and depth of penetration compared to confocal microscopy [3]. FFOCT has been used for diagnosis of fixed and non-fixed tissue samples for the detection of breast, lung and skin and ovarian tissues [4, 5].

Morphological heterogeneity of tumor tissue has recently emerged as an import diagnostic parameter [6]. Morphological analysis, which involves detecting changes in the gray level intensity of a medical image, has been successfully used for differentiating between normal and malignant pathologies using several imaging modalities, such as Ultrasound, MRI and Spatial frequency domain imaging. [7-9]. Several approaches of texture analysis have been demonstrated. These include statistical methods such as histogram analysis, mathematical model-based approach including fractal analysis as well as transform based methods including Wavelet, Fourier and Gabor transform. Conventional OCT has also been applied for texture analysis of tissues, however, all the imaging modalities explored are difficult to compare with high resolution H&E stained histology images [10-14]. Histology, which can provide microscopic tissue information with high degree of accuracy, is currently limited by staining methods and an extended diagnosis wait time and often require repeated visits for the patient. FFOCT on the other hand can provide rapid high resolution, label-free images of tissues with comparable accuracy. So far, most of the studies on FFOCT have relied on visual observation of normal and malignant structures. This limits the interpretation across different observers and may affect the ultimate diagnosis. Automated image analysis methods can provide a robust and accurate method independent of visual interpretation limitations. In this work, we have explored the initial feasibility of using a FFOCT system for imaging and analysis of human ovarian tissue samples. Five features were quantitatively extracted from normalized histogram of the normal and malignant images. These were the mean, standard deviation, entropy, skewness and kurtosis. The sensitivity, specificity as well as the area under the receiver operating (ROC) curve (AUC) was evaluated for diagnostic accuracy. To the best of our knowledge, this is the first ever study to report the quantitative morphological analysis and feature extraction using FFOCT for classification of normal and malignant human ovarian tissue. Quantitative information from FFOCT images can be invaluable for physicians for high resolution, label free, rapid diagnosis of neoplastic changes related to ovarian cancer [15].

3.2 Materials and Methods

3.2.1 Ovary Sample

De-identified formalin fixed paraffin embedded (FFPE) tissue blocks of human ovarian tissue samples were acquired from University of Massachusetts (UMass) Memorial Cancer Center and University of Connecticut Health Center (UCHC). After imaging, the slides corresponding to the imaged planes were identified, and stained using hematoxylin and eosin (H&E) for diagnosis.

3.2.2 FFOCT System

Figure 3.1 shows the configuration of the FFOCT system, which is based on a Linnik interferometer consisting of two objective lenses (10X, N.A. 0.25), one each in the reference and sample arm. A 6 V, 20 W halogen lamp (central wavelength 560 nm, bandwidth 200 nm) customized with Köhler illumination was used to illuminate the sample. The reference mirror was connected to a piezo stage (Thorlabs, NF5DP20) and the samples were placed on a 3d stage. The en face interferometric images were captured by a 12-bit CCD camera (Basler acA1300-30um, 1296 x 966 pixels, 30 fps). The axial resolution of the system was measured from the FWHM of the axial PSF to be 1.6 μm and the lateral resolution was measured by imaging a sharp edge, and was around 6 μm.

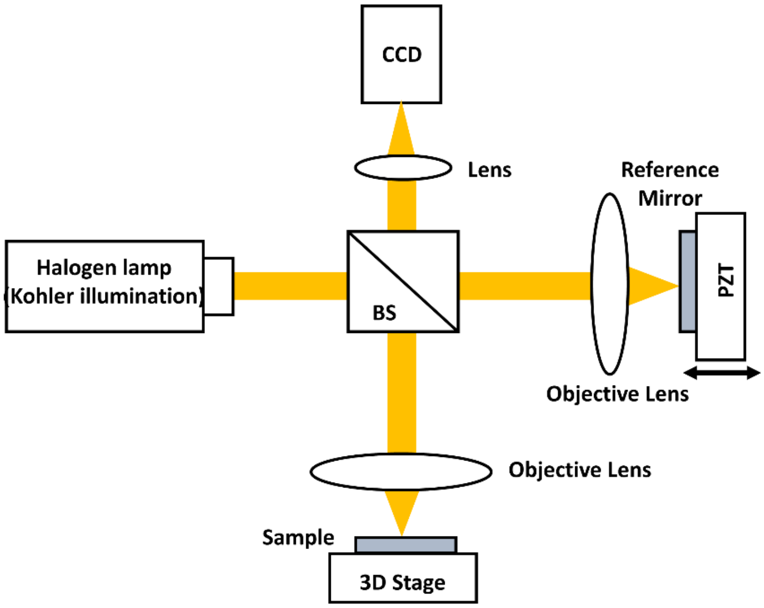

Figure. 3.1 FFOCT system configuration. Set up of the FFOCT system.

3.2.3 FFOCT Imaging Procedure

FFPE ovarian tissue blocks were placed on a 3d stage and four phase-shifted en face images were acquired with the CCD camera, from which the OCT image was computed using a derivative algorithm. The field of view was 0.8 cm x 0.8 cm. The depth of penetration was around 100 µm. Overall acquisition time for each location was 0.3 seconds. The OCT images were then compared with the H&E slides by a trained pathologist for identification of benign and malignant features corresponding to ovarian cancer metastasis.

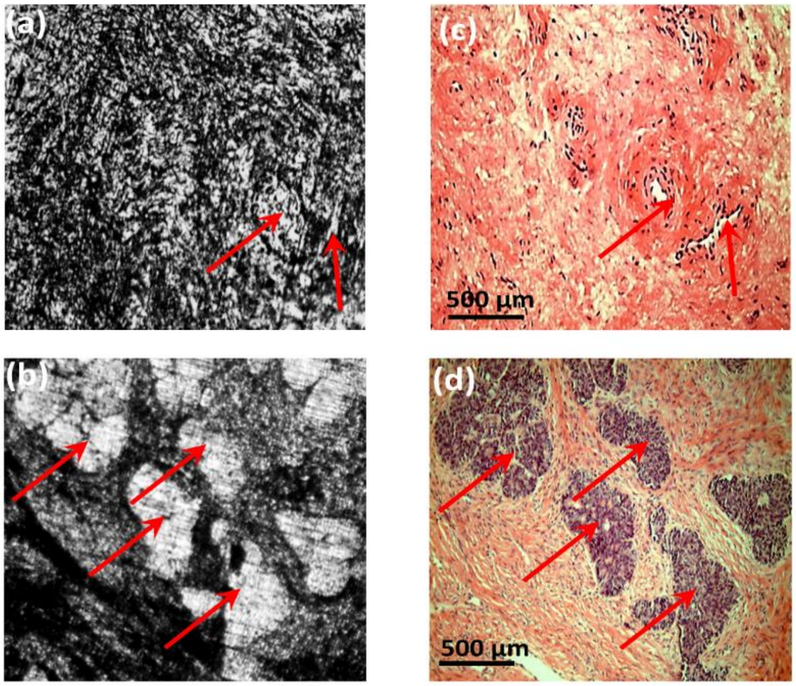

Figure. 3.2. FFOCT Images. (a) normal and (b) malignant ovary; corresponding H&E histology images are shown in (c, d). The matching areas indicated by red arrows.

3.2.4 Feature Extraction

Each image (0.8 cm x 0.8 cm) was further divided into several non-overlapping sub images (0.1 cm x 0.1 cm), based on the pathologists' observation of normal and malignant structures. Five features were extracted quantitatively using MATLAB from the analysis of the normalized histogram of these normal and malignant FFOCT ovary images. These were mainly based on the observed differences in the morphology of the two ovarian tissue groups. The five features are the mean pixel intensity, variance, entropy, skewness and kurtosis of the image histogram. Entropy was used to signify the irregularity of the gray level distribution, and the deviation of the histogram distribution was calculated from the variance. Kurtosis and skewness signified the flatness and asymmetry of the image histogram. It was assumed that identification of one image from a sample as cancer was sufficient to classify the ovary as malignant, and only if every image from a sample was found to be normal then the ovary was considered normal [16]. In general, lower mean value of an image combined with higher values of variance, entropy, skewness and kurtosis signified increased heterogeneity of the image, which can be associated with development and progression of cancer. A logistic regression model was used to classify the normal and malignant ovarian tissue groups. The five features extracted from FFOCT images were used as predictor variables, and response variable was the actual diagnostic results (1 representing malignant and 0 representing normal). The coefficients of the linear model were determined by MATLAB GLMFIT function and then the same set of coefficients were applied to MATLAB GLMVAL function to calculate the responses of the testing set. The quality of the model was evaluated using receiver operating curve (ROC) and the area under the curve (AUC).

3.3 Results and Discussions

A total of 14 ovarian tissue samples were imaged *ex vivo* with the FFOCT system, consisting of 7 benign and 7 malignant samples. The malignant tissue samples consisted of various grades of serous carcinoma, which is the most common type of epithelial ovarian cancer, as well as cases of endometroid and mucinous carcinoma. Fig 3.2 shows the FFOCT images of a normal and malignant ovarian tissue along with the corresponding H&E stained histology images. It can be observed from the FFOCT and histology images that normal ovarian tissue has visibly smoother and homogeneous stroma with dense collagen distribution, while the malignant ovary has highly degenerated, fragmented and heterogeneous stroma, characterized by poorly differentiated and clustered tumor architecture.

Five features were extracted from normalized histogram of 105 non-overlapping FFOCT images (57 normal and 48 normal). Figure 3.3 shows the boxplot and p values of the features normalized mean, variance, kurtosis, skewness and entropy. It can be observed from Fig 3.3 that the malignant tissue group has lower mean intensity value compared to the normal group, which may be attributed to aggravated necrosis and reduced collagen concentration. Additionally, the variance, kurtosis, skewness and entropy of the group of malignant ovaries were significantly higher, signifying more heterogeneity and clustering associated with development of cancer.

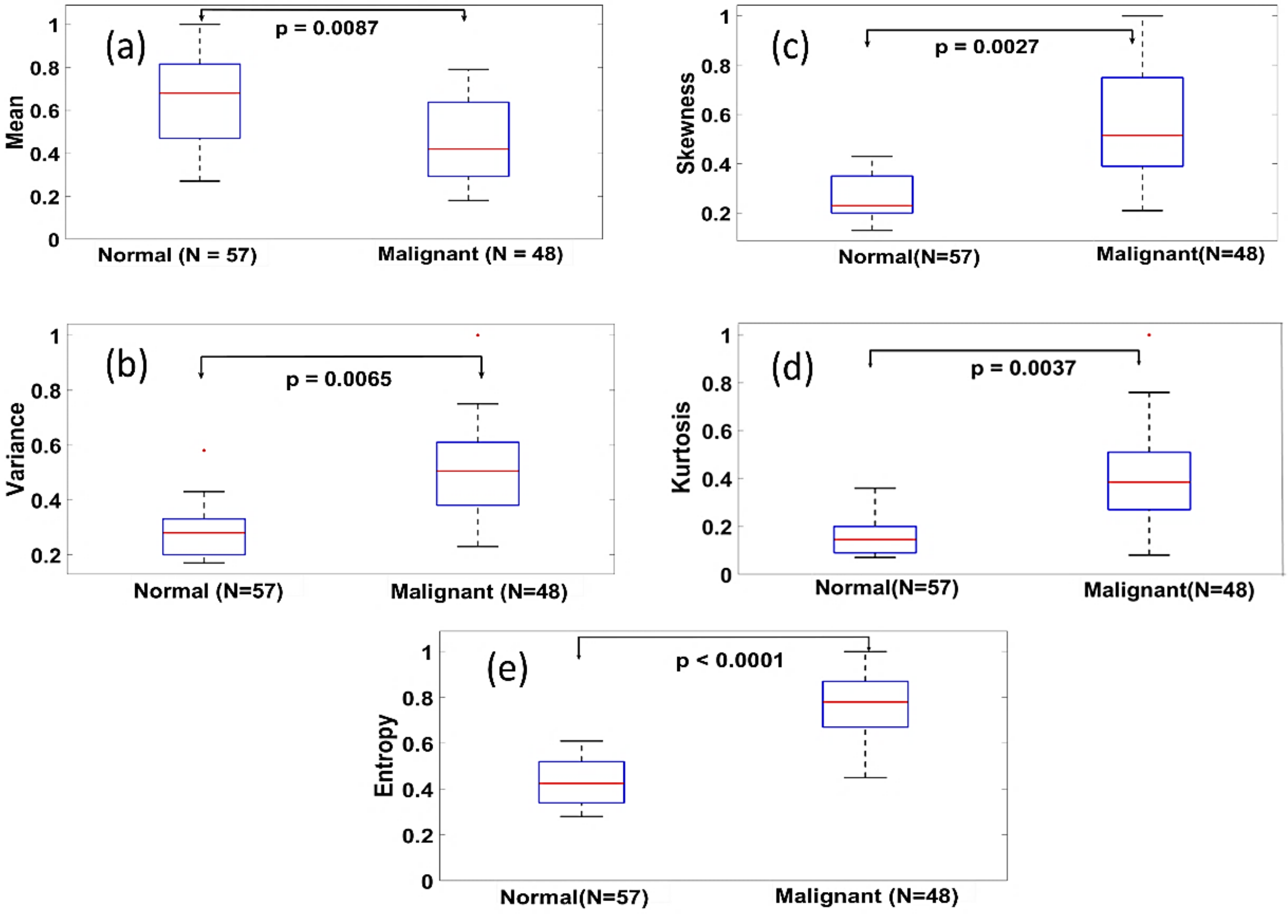

Figure. 3.3 Statistics of features. Boxplot of the five features along with the p values for (a) mean, (b) variance, (c) skewness, (d) kurtosis and (e) entropy.

For classification between normal and malignant ovarian tissue groups, the images were separated into two groups, 60 images were used for training (32 normal, 28 malignant) the logistic classifier and 45 images (25 normal, 20 malignant) were tested using the logistic regression model. Figure 4 shows the ROC curves for both the training and testing sets. For the training set, a sensitivity and specificity of 94.6% and 90.4% was obtained, with average AUC at 95% confidence interval being 0.968, while for the testing set, we obtained a sensitivity of 92.2% and specificity of 87.3%, with average AUC of 0.895 at 95% confidence interval.

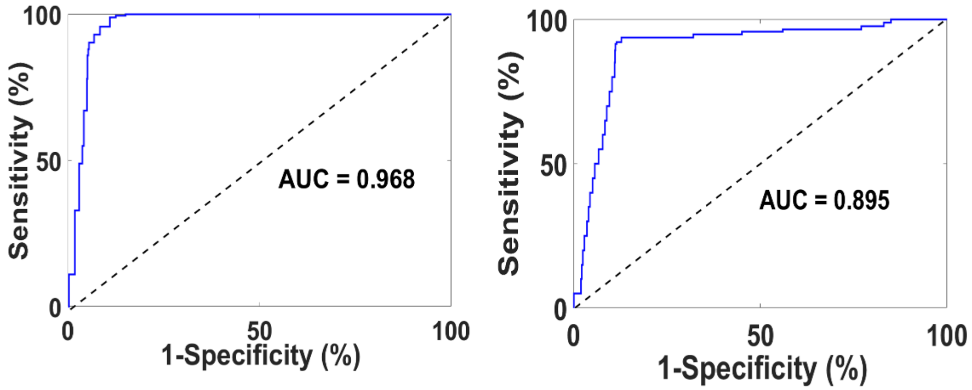

Figure. 3.4 ROC curve. (a) training and (b) testing sets using the five features.

The current work has several limitations. The training and testing results are based on a limited sample pool, and more data needs to be acquired for further validation. Additionally, only FFPE tissue blocks were used for this preliminary study. Although, previous imaging studies indicate that classification of fresh and FFPE tissues produce comparable results, however, further compatibility studies need to be conducted between these two tissue groups [17]. Also, a lower NA objective lens was used, and much higher cellular level transverse resolution can be obtained by using high NA objective lenses, as shown by previous FFOCT studies. The current study in intended to be implemented as a rapid *ex vivo* alternative for conventional H&E based histology, which require staining and long diagnostic wait times. The idea is to take a biopsy sample of the tissue and make a rapid optical diagnosis of normal and malignant tissues based on FFOCT images, which is comparable in resolution to standard histology methods and also does not require extensive staining methods. Future work will include studying freshly excised tissue samples and incorporating the data processing and feature extraction methods in real time, so that the technology can be transferred from bench to bedside.

3.4. Summary

In this study, 14 human ovarian tissue samples were imaged *ex vivo* using the FFOCT system, and five quantitative features were extracted from the normal and malignant ovarian tissue images. Using a logistic classifier model, a sensitivity of 92.2% and specificity of 87.3% was achieved. The initial promising results indicate that FFOCT can potentially be a very useful diagnostic tool for label free, rapid and low cost quantitative analysis of the ovarian tissue and reduce the wait times associated with conventional histology.

References

[1] Dubois A., Vabre L., Boccara A. C., and Beaurepaire E., “High-resolution full-field optical coherence tomography with a Linnik microscope,” Appl. Opt. 41(4), 805–812 (2002).

[2] Dubois A. and Boccara A. C., “Full-field optical coherence tomography” in Optical Coherence Tomography, E.D. W. Drexler and J. G. Fujimoto, eds. (Springer, 2009), pp. 565–591.

[3] Aguirre A. D., Sawinski J., Huang S.W., Zhou C., Denk W., and Fujimoto J. G., “High speed optical coherence microscopy with autofocus adjustment and a miniaturized endoscopic imaging probe,” Opt. Express 18(5), 4222–4239 (2010).

[4] Assayag O. et al, “Large Field, High Resolution Full-Field Optical Coherence Tomography: A Preclinical Study of Human Breast Tissue and Cancer Assessment,” Technol. Cancer Res. Treat. 13(5), 455–468 (2014).

[5] Jain M. et al, “Full-field optical coherence tomography for the analysis of fresh unstained human lobectomy specimens,” J. Pathol. Inform. 4(26), 26 (2013).

[6] Davnall F. et al, "Assessment of tumor heterogeneity: an emerging imaging tool for clinical practice?" Insights Imaging 3(6), 573–589 (2012).

[7] Holli K. et al, "Characterization of breast cancer types by texture analysis of magnetic resonance images," Acad. Radiol. 17(2), 135–141 (2010).

[8] **Nandy S.**, Mostafa A., Kumavor P. D., Sanders M., Brewer M., and Zhu Q., "Characterizing optical properties and spatial heterogeneity of human ovarian tissue using spatial frequency domain imaging," J. Biomed. Opt. 21(10), 101402 (2016).

[9] Tuceryan M. and Jain A. K., "Texture analysis. In: Chen CH, Pau LF, Wang PSP, editors. The Handbook of Pattern Recognition and Computer Vision," World Scientific Publishing Co., pp. 207–248 (1998).

[10] Lopes R., Ayache A., Makni N., Puech P., Villers A., Mordon S., and Betrouni N., "Prostate cancer characterization on MR images using fractal features," Med. Phys. 38(1), 83–95 (2011).

[11] Brown R. A. and Frayne R., "A comparison of texture quantification techniques based on the Fourier and S transforms," Med. Phys. 35(11), 4998–5008 (2008)

[12] Gossage K. W., Tkaczyk T. S., Rodriguez J. J., and Barton J. K., "Texture analysis of optical coherence tomography images: feasibility for tissue classification," J. Biomed. Opt. 8(3), 570–575 (2003).

[13] Castellano G., Bonilha L., Li L. M., and Cendes F., "Texture analysis of medical images," Clin. Radiol. 59(12), 1061–1069 (2004).

[14] Chen D. R., Chang R. F., and Huang Y. L., "Computer-aided diagnosis applied to US of solid breast nodules by using neural networks," Radiology 213(2), 407–412 (1999).

[15] **Nandy S.**, Sanders M., and Zhu Q., “Classification and analysis of human ovarian tissue using full field optical coherence tomography,” Biomed. Opt. Express 7(12), 5182–5187 (2016).

[16] Alqasemi U., Kumavor P., Aguirre A., and Zhu Q., “Recognition algorithm for assisting ovarian cancer diagnosis from coregistered ultrasound and photoacoustic images: ex vivo study,” J. Biomed. Opt. 17(12), 126003 (2012).

[17] Ly A. et al, “High-mass-resolution MALDI mass spectrometry imaging of metabolites from formalin-fixed paraffin embedded tissue,” Nat. Protoc. 11(8), 1428–1443 (2016).

Chapter 4 Spatial Frequency Domain Imaging (SFDI) For Quantitative Assessment of Normal and Malignant Human Ovarian and Colon Pathologies

4.1 Background

Spatial frequency domain imaging (SFDI) is an emerging imaging modality for surface mapping of wide field tissue optical properties, e.g. absorption, scattering, total blood hemoglobin (HbT) and oxygen saturation (% sO_2) over a large field of view. Sinusoidal illumination patterns are projected on the ovarian tissue surface and the diffused reflection image is captured by a CCD camera. The sinusoidal illumination pattern can be expressed as:

$$\mathrm{I} = \mathrm{I_0} \sin(2\pi \mathrm{f_x} \mathrm{x} + \alpha) \qquad (4.1)$$

Where $\mathrm{I_0}$ is the incident source intensity, $\mathrm{f_x}$ is the spatial frequency and α is the phase. Three phase shifted images ($\mathrm{I_1}, \mathrm{I_2}$ and $\mathrm{I_3}$) were recorded (α = 0, 120 and 240 degrees) for each frequency and the demodulated DC and AC components were obtained by the formulae:

$$\mathrm{M_{DC}} = \frac{\mathrm{I_1}+\mathrm{I_2}+\mathrm{I_3}}{3} \qquad (4.2)$$

$$\mathrm{M_{AC}} = \frac{\sqrt{2}}{3}\left[(\mathrm{I_1}-\mathrm{I_2})^2 + (\mathrm{I_3}-\mathrm{I_2})^2 + (\mathrm{I_3}-\mathrm{I_1})^2\right]^{1/2} \qquad (4.3)$$

However, $\mathrm{M_{DC}}$ term is affected by the system noise e.g. the dark current as well as the ambient light. Hence, the frequency dependent component $\mathrm{M_{AC}}$ was calculated for each spatial frequency to cancel out the common mode system noise and calibrated with a phantom of known optical properties using the forward light transport model to yield measured reflectance R_D (f_x). Using only two frequencies, the optical absorption and scattering of the tissue can be recovered. Multiple wavelengths can be used to recover important wavelength dependent parameters such as HbT, sO_2, and wavelength dependent tissue scatter amplitude and scatter spectral slope, which are important diagnostic parameters for detecting neoplastic changes in the human ovarian tissue. Two versions of the system have been used, the first one used a bulky commercial projector and a single wavelength (730nm) [1]. The second version used a miniaturized Pico projector and multiple visible wavelengths (460 nm, 530 nm and 630 nm) [2]. A third version which can be used as a handheld, portable device is currently under development.

4.2 Materials and Methods

4.2.1 First Generation SFDI System

The configuration of the SFDI imaging system is shown in Figure 1. Sinusoidal patterns were projected using an automated Microsoft PowerPoint presentation, from a DLP projector (XD430U, Mitsubishi) consisting of a 0.55-in. single-chip digital micro mirror device and a 230-W Tungsten Halogen lamp. The RGB color wheels were removed to provide uniform illumination on the sample. The projector was turned on for 10 min before the experiments for stabilizing the source. The diffuse reflected light was captured by a camera (Edmund Optics USB EO-0413M 1/3” CMOS Monochrome, 8 bit, 752 × 480 pixels, dynamic range > 55 dB linear) synchronized with the projection system and capable of imaging up to 87 frames per second. The illumination area was 7 cm × 7 cm, while the FOV captured by the camera was 4 cm × 4 cm. The tissue samples were placed with respect to the camera in a way to cover most of the FOV to avoid light leakage from the sides. A laser line filter (Thorlabs FL730-10, CW 730 nm, BW ± 10 nm) was attached to the camera. The specular reflection was minimized by using two crossed linear polarizers (Edmund Optics, polarization efficiency > 99%), and a small angle of incidence (15 degrees to the normal). Previous studies on spectroscopic characterization of human ovarian tissue have been performed mainly in the wavelength range of 390 to 600 nm using reflectance spectroscopy, and 700 to 900 nm by using photoacoustic tomography, but these studies are limited in providing the absolute quantitative values of tissue absorption and scattering. As an initial pilot study, the wavelength of 730 nm was selected, mainly because of previous extensive knowledge and data of malignant and benign ovarian tissue absorption or vasculature obtained from photoacoustic tomography studies in this wavelength range [3]. Also, this wavelength was available for comparison of accuracy of phantoms from our previous frequency domain (FD) diffuse light imaging system [4]. The overall acquisition time was ≈ 1 min, which makes the system suitable for *ex vivo* evaluation of the ovary. To minimize the effect of ambient light, the system was located in a dark room, and the laser line filter attached to the camera accepted only narrowband illumination.

The diffuse reflectance varies exponentially with the square of the distance (h) between the camera and the object and a height offset between the sample and reference calibration can affect the measured reflectance, introducing errors in both μ_a and μ_s'. The distance between the camera and the reference phantom was adjusted to be 12 cm, while for imaging the phantom and tissue samples, the height offset was carefully adjusted with an x-y-z stage to within 1mm, which had negligible scaling effect on the measured diffuse reflectance [5]. The penetration depth δ_{eff} in the spatial frequency domain, depends on the effective attenuation coefficient, $\mu_{eff} = \sqrt{3\mu a(\mu a + \mu' s)}$ and the spatial frequency f_x, where $\mu'_{eff} = [\mu^2_{eff} + (2\pi f_x)^2]^{1/2} = [\delta eff]^{-1}$ [6].

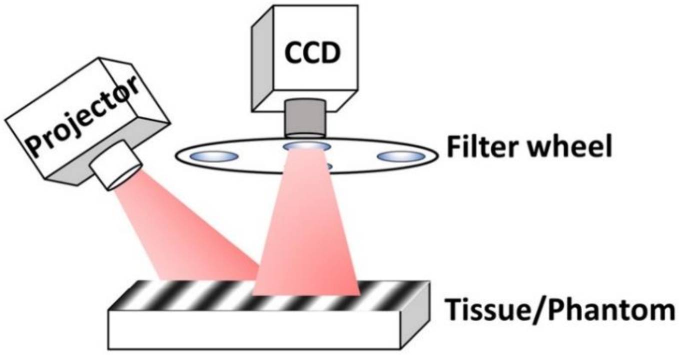

Figure. 4.1 SFDI system. SFDI system setup.

4.2.2 Second Generation Miniaturized Multispectral SFDI System

In the previous section, a single wavelength SFDI system with a bulky projection unit was used to image differences in absorption, scattering as well as spatial heterogeneities between benign and malignant ovarian tissues. For the next generation SFDI system, we used a multispectral SFDI system with a miniaturized projector at visible wavelengths for *ex vivo* quantification of wavelength dependent chromophores as well as spatial heterogeneities of freshly excised benign and malignant human ovarian and colon tissues. Sinusoidal patterns generated in MATLAB were projected from a miniaturized Pico projector (RIF6 cube, dimension 2”x2”x1.9”, brightness 50 lumens), and the diffuse reflected light was recorded by a 12 bit CCD camera (Basler ace, 30 fps, dynamic range 57 dB) and bandpass filters (Thorlabs, bandwidth ± 10 nm). Three wavelengths (460 nm, 530 nm and 630 nm) and two optimized spatial frequencies (0 and 1 cm^{-1}) were used for this study. The specular reflection was minimized by two crossed linear polarizers. The field of view (FOV) captured by the camera was same as before, i.e. 4 cm x 4 cm.

4.2.3 Calculation of Spatial and Spectral Features

Depending on the size of the tissue sample, several nonoverlapping images were recorded for each sample, and subsequently each SFDI absorption and scattering image was subdivided into independent regions of interest of same size for extracting the spectral and spatial features. Four features were quantitatively extracted from the observed differences between the wavelength-dependent absorption and scattering properties. These were the total hemoglobin (HbT), oxygen saturation (sO_2), scatter amplitude and scatter spectral slope. HbT and sO_2 are important prognosticators of angiogenesis and oxygen consumption, respectively, which are related to tumor progression. The scatter amplitude was proportional to the concentration of elastic scatterers, mainly collagen. The scatter spectral slope was related to the size of the scatterers, with higher slope indicating the presence of smaller collagen fibrils that enhanced Rayleigh-type scattering [7]. Additional features related to the spatial heterogeneity of absorption and scattering were extracted from taking the Radon transform of the absorption and scattering maps, and correspondingly fitting the average profile to a gaussian function.

To determine the strength of association between each SFDI feature and the histology of the imaged specimen, logistic regression model was used. All statistical tests were performed using MATLAB version 2016. The spectral and spatial features were used as predictor variables, and the diagnosis from pathology was used as response variable (0 for normal, 1 for cancer). The receiver operating curve (ROC) and the area under the curve (AUC) was used to test the performance accuracy of the logistic classifier.

4.2.4 Human Ovary Sample Study

Human ovarian tissue samples were obtained from patients undergoing PO at the University of Connecticut Health Center (UCHC), and Washington University School of Medicine (WUSM). This study was approved by the Institutional Review Boards (IRB) of UCHC and WUSM, and informed consent was obtained from all patients. The overall imaging was completed within a 1 hour time window from the time of surgery, to avoid excessive blood loss and changes in physiological properties. During the surgery, ovaries were surgically cut from the side of the Fallopian tube, so as to leave no incision mark on the ovary surface, which might affect the diagnosis. For the first-generation system, 15 *ex vivo* ovaries (8 premenopausal, 7 post-menopausal which included 5 normal and 2 malignant) from 9 patients were studied. For the next generation system, we imaged a total of 14 intact ovaries (10 normal/benign, 4 malignant) from 11 patients using the SFDI system. The non-cancerous samples consisted of 2 normal and 8 enlarged but benign ovaries. The diagnoses for the benign ovarian masses consisted of cystic ovaries and fibro thecoma. The malignant samples consisted of a borderline serous tumor, two endometroid adenocarcinomas and a high-grade serous carcinoma. Most of the benign ovaries (9 ovaries) for this set were from post-menopausal patients, while all the malignant ovaries were from pre-menopausal patients. The borderline tumor was included in the malignant category due to the clinical impact of this diagnosis. After the imaging, the ovaries were fixed in 10% formalin solution and returned to the Pathology Department for histological processing.

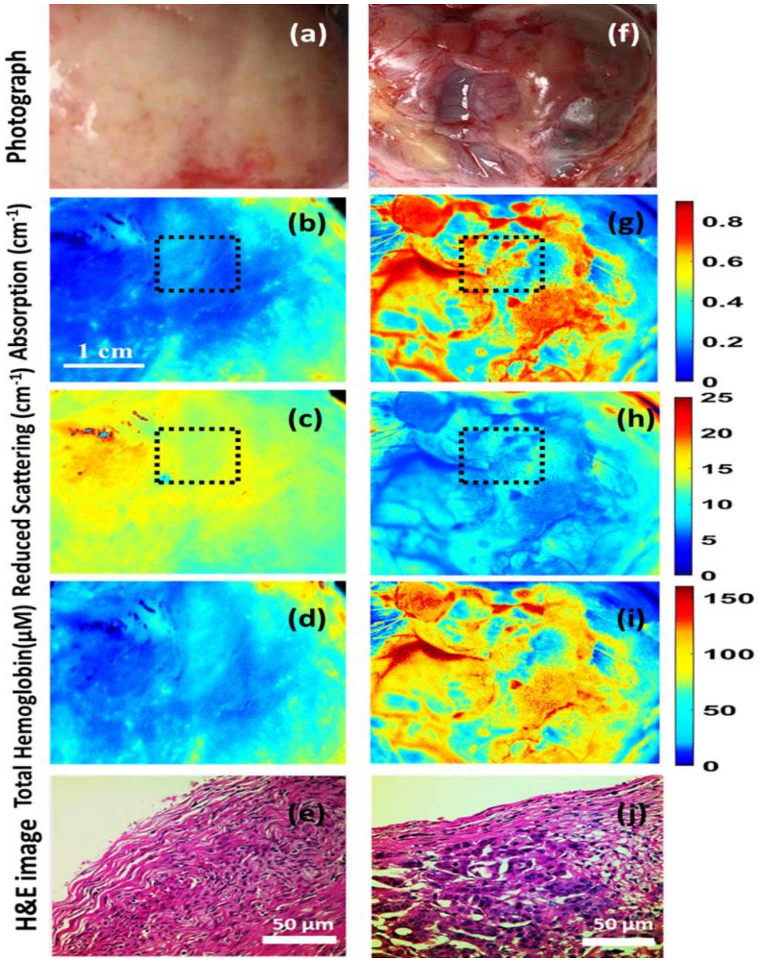

Figure. 4.2 SFDI results for human ovary. Color photograph, absorption, reduced scattering (530 nm), total hemoglobin map, H&E image from representative areas of a benign fibro thecoma (a-e) and a high-grade serous carcinoma (f-j); Black dashed area showing the ROI for feature selection.

4.2.5 Ovary Study Results

It was observed that the malignant ovaries had significantly higher total hemoglobin as well as lower scatter amplitude and slope. This may be due to increased angiogenesis and lack of elastic scatterers such as stromal collagen in the malignant ovarian tissue compared to the non-cancerous ovaries, as evident in the H&E images from the imaging areas of benign and malignant ovaries. Additionally, the absorption and scatter heterogeneity were also highest for the malignant group, signifying clustered, random distribution of micro vessels as well as scattered collagen distribution. The SD of the Gaussian fitting function was also found to be significantly lower for the malignant group as compared to the normal group. In terms of statistical significance, HbT was found to be the most important feature, followed by scatter slope, scatter amplitude, absorption heterogeneity, absorption SD, scatter heterogeneity and scatter SD. Oxygen saturation was not found to be a significant *ex vivo* feature (p = 0.53).

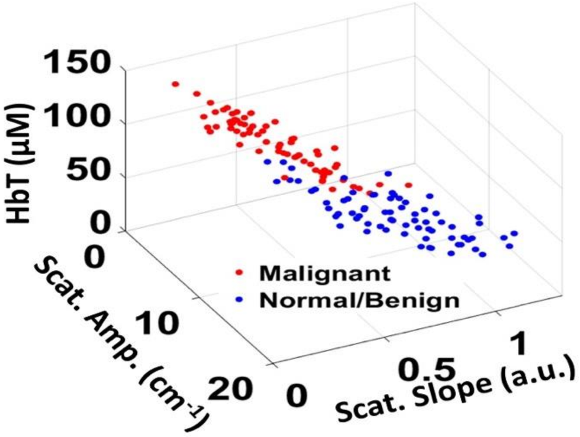

Figure. 4.3 Spectral feature plot. Scatter plot of spectral features of Normal/Benign and Malignant ovaries.

ROC curves and AUC of the training and testing set using the spatial and spectral features are shown in Fig. 4.4. For the training set, we obtained sensitivity 97.69%, specificity 96.97%, PPV 96.21%, NPV 97.97% and AUC (95% confidence interval) of 0.985. For the testing set, we obtained sensitivity 94.06%, specificity 93.53%, PPV 92.23%, NPV 95.04% and AUC (95% confidence interval) of 0.938.

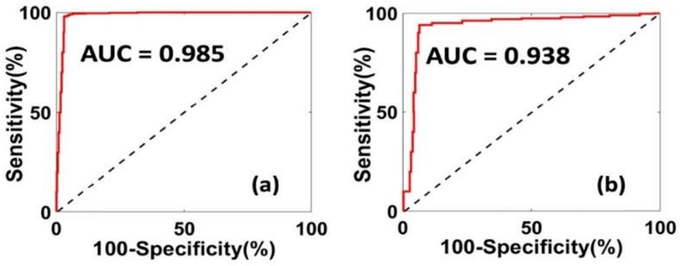

Figure. 4.4 ROC curves. (a) Training; (b) Testing.

4.2.6 Human Colon Sample Study

Freshly resected colon samples obtained from patients undergoing surgery at Washington University School of Medicine were imaged immediately after surgery. The study was approved by the Institutional Review Board (IRB) at Washington University, and informed consent was obtained from all patients. The majority of patients underwent hemicolectomy for cancer and were found to have malignancy on histologic analysis. Each specimen was opened longitudinally in the operating room, rinsed with sterile water to remove any blood or debris from the mucosal surface, and secured to backing with pins. This exposed the mucosal surface of the organ for imaging. Immediately upon completion of imaging, the samples were placed in formalin and returned to the pathology department for histological processing. A total of 9 patients enrolled in the pilot study, and 15 (8 malignant, 7 normal) regions were imaged using the SFDI system.

4.2.7 Colon Study Results

In general, malignant colon tissue demonstrated several distinct features compared to normal tissue when imaged with SDFI. HbT concentrations tended to be elevated in tumors, while light scattering tended to be significantly decreased, with reduced scatter amplitude and scatter spectral slope. Additionally, tumor tissue was highly heterogeneous and unorganized with significant intra-tumor variation of both absorption and scattering.

The drastic alteration in the mucosal morphology was evident in the neoplastic colon tissues, with no regularity of pattern, in comparison to normal tissue, which showed regular, homogenous patterned structure of mucosa and submucosa. The disruption of the normal mucosal and submucosal structure due to invasive carcinoma was also confirmed from the histology images.

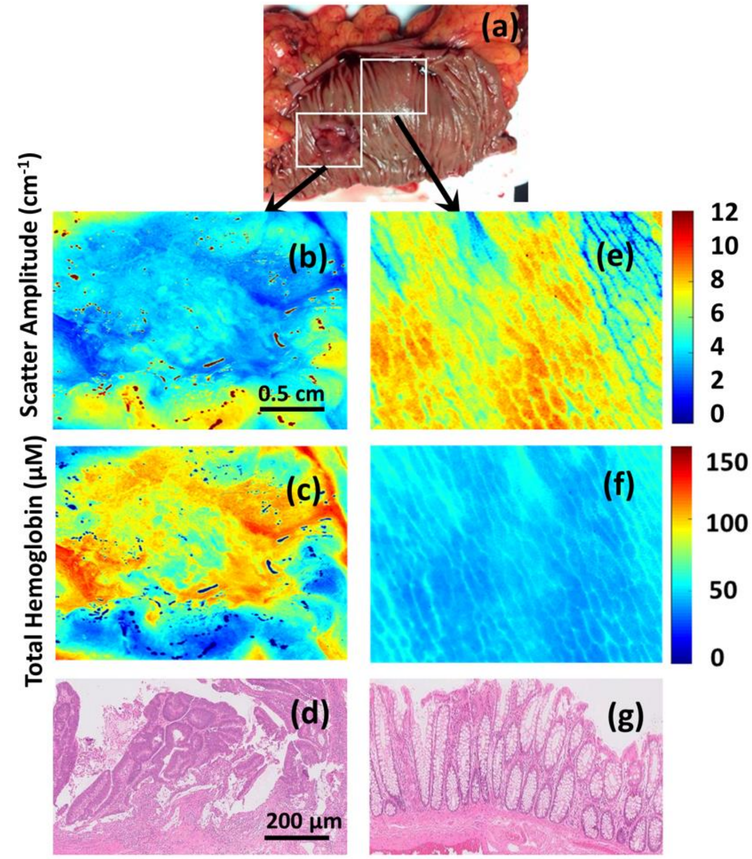

Figure. 4.5 SFDI colon results. Photograph, scatter amplitude map and total hemoglobin (HbT) map of a moderately differentiated adenocarcinoma (Images b-d) and corresponding normal tissue (images e-g).

Using the SFDI spectral and spatial features, the Receiver Operator Curve (ROC) demonstrated an optimum sensitivity of 90.91%, specificity of 88.89% and accuracy of 90%, and the mean AUC was 0.902.

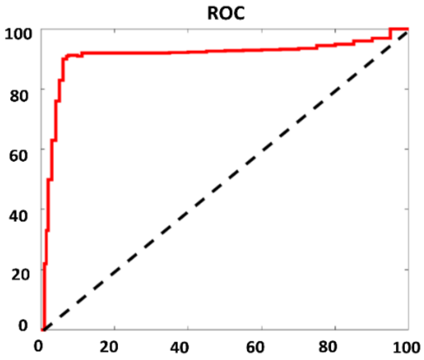

Figure. 4.6 ROC curve. Testing ROC using logistic model for all five features

4.3 Summary

The feasibility of SFDI as a label free, rapid, wide field, multispectral evaluation tool for discrimination of benign and malignant tissue pathologies was demonstrated. Significant differences in optical absorption and scattering properties were observed between normal and malignant ovarian as well as between normal and neoplastic colon tissues, along with drastically different morphological features. Currently, a handheld, multispectral SFDI probe is under development that can transform the SFDI technology from bench to the bedside and provide the surgeons an effective evaluation and monitoring of normal and diseased tissues.

References

[1] **Nandy S**, Mostafa A, Kumavor P. D., Sanders M., Brewer M., and Zhu Q., “Characterizing optical properties and spatial heterogeneity of human ovarian tissue using spatial frequency domain imaging,” J. Biomed. Opt. 21(10), 101402 (2016).

[2] **Nandy S.**, Hagemann I. S., Powell M. A., Siegel C., and Zhu Q., "Quantitative multispectral ex vivo optical evaluation of human ovarian tissue using spatial frequency domain imaging," Biomed. Opt. Express 9(5), 2451–2456 (2018).

[3] Utzinger U., et al., “Reflectance spectroscopy for in vivo characterization of ovarian tissue,” Lasers Surg. Med. 28(1), 56–66, (2001).

[4] Xu C., et al., “Ultrasound-guided diffuse optical tomography for predicting and monitoring neoadjuvant chemotherapy of breast cancers: recent progress,” Ultrason. Imaging 38(1), 5–18 (2015).

[5] Bodenschatz N., Brandes A., Liemert A., and Kienle A., “Sources of errors in spatial frequency domain imaging of scattering media,” J. Biomed. Opt. 19(7), 071405 (2014).

[6] Cuccia D. J., Bevilacqua F., Durkin A. J., Ayers F. R., and Tromberg B. J., “Quantitation and mapping of tissue optical properties using modulated imaging,” J. Biomed. Opt. 14(2), 024012 (2009).

[7] Jacques S. L., “Optical properties of biological tissues: a review,” Phys. Med. Biol. 58(11), R37–R61 (2013).

Chapter 5 Co-Registered Photoacoustic Tomography with Ultrasound (PAT/US) for *In Vivo* Imaging of Human Ovarian Cancer

5.1 Background

In vivo diagnosis and detection of ovarian cancer remains a challenge due lack of early symptoms, as well as limitations of current screening modalities such as ultrasound (US), computed tomography (CT), magnetic resonance imaging (MRI), as well as other methods such as serum marker 125 (CA-125) and pelvic examination provide low specificity for early stage detection of ovarian cancer [1-3]. A crucial need exists to develop *in vivo* functional imaging modalities that can detect ovarian cancer at an early stage with considerable accuracy.

Photoacoustic tomography (PAT) has recently emerged as a powerful tool for *in vivo* functional imaging ranging from the depth of couple of millimeters to several centimeters inside the tissue with considerable spatial resolution. PAT uses a short-pulsed laser to excite tissue, that generate photoacoustic waves, which are then measured by US transducers and subsequently used to image the optical absorption distribution. The optical absorption at NIR (600-900 nm) wavelengths is directly proportional to the blood vasculature and thus to tumor angiogenesis, which is a key process for tumor growth and metastasis. Using two or more wavelengths, photoacoustic oxygen saturation (sO_2) can then be measured, which is an important indicator of tumor metabolism and therapeutic response [4, 5].

Previous applications of PAT in oncology include breast cancer [6], prostate cancer [7], skin cancer [8], thyroid cancer [9] and ovarian cancer [10].

The current study was focused on functional multispectral *in vivo* imaging of suspected ovarian cancer patients using co-registered photoacoustic tomography and pulse-echo ultrasound (PAT/US).

5.2 Materials and Methods

5.2.1 PAT/US Imaging System

The imaging system consisted a fully programmable clinical US system (EC-12R, Alpinion Medical Systems, Republic of Korea), a customized optical fiber- based light delivery system coupled with a transvaginal US probe, and a Nd:YAG laser pumped pulsed (10 ns, 15 Hz), tunable (690-900 nm) Ti-sapphire laser (Symphotics, Camarillo, California). Each PAT and US frame were synchronized, and four wavelengths (730 nm, 780 nm, 800 nm and 830 nm) were used for multispectral imaging.

5.2.2 Ovarian Patient Study

Patients who had a suspected ovarian mass or risk of developing ovarian cancer, were enrolled for the current study. The subjects were consented, and the study was approved by IRB at WUSM. All patients were initially examined with a commercial US system by a trained radiologist, and subsequently the same area was imaged by the co-registered PAT/US system. Functional parameters such as relative total hemoglobin ($rHbT$) and oxygen saturation (sO_2) were computed. CA-125, a blood marker was available for most of the patients, and its performance was compared with the functional photoacoustic features.

5.3 Results and Discussions

A total of 20 patients consented for the study, out of which 16 patients (26 ovaries) were imaged using the PAT/US system. Subsequent surgical pathology diagnosis revealed that the malignant ovaries consisted of high grade serous carcinoma (n=6), endometroid adenocarcinoma (n=3) and other types of borderline and sex-chord stromal tumors (n=3). The other group consisted of normal (n=3) and benign (n= 9) ovaries.

Figure 5.1 shows on of the results obtained from the co-registered PAT/US imaging. The patient had an enlarged right adnexal mass (Figure 5.1. a-b) which shows extensive and diffused vasculature as well as elevated total hemoglobin level and reduced oxygen saturation, which is drastically different from the scattered and lower signal level and elevated oxygen saturation level observed in the left ovary of the same patient (Figure 5.1.d-e). The surgical pathology diagnosis of the right ovary revealed well differentiated endometroid adenocarcinoma (Figure 5.1 c), while the left ovary was found to have no histopathological abnormalities (Figure 5.1 d).

The average *rHbT* was 1.9 times higher for invasive epithelial cancers than for the benign and normal ovaries. Additionally, the *rHbT* distribution was extensive in invasive epithelial cancers, but was scattered in benign and normal ovaries. The *rHbT* of two borderline serous tumors and one stromal tumor was in the same range as that of benign and normal ovaries. The mean sO_2 of invasive epithelial cancers, as well as of the borderline and stromal tumors, was significantly lower (8.2%) than that of benign and normal ovaries.

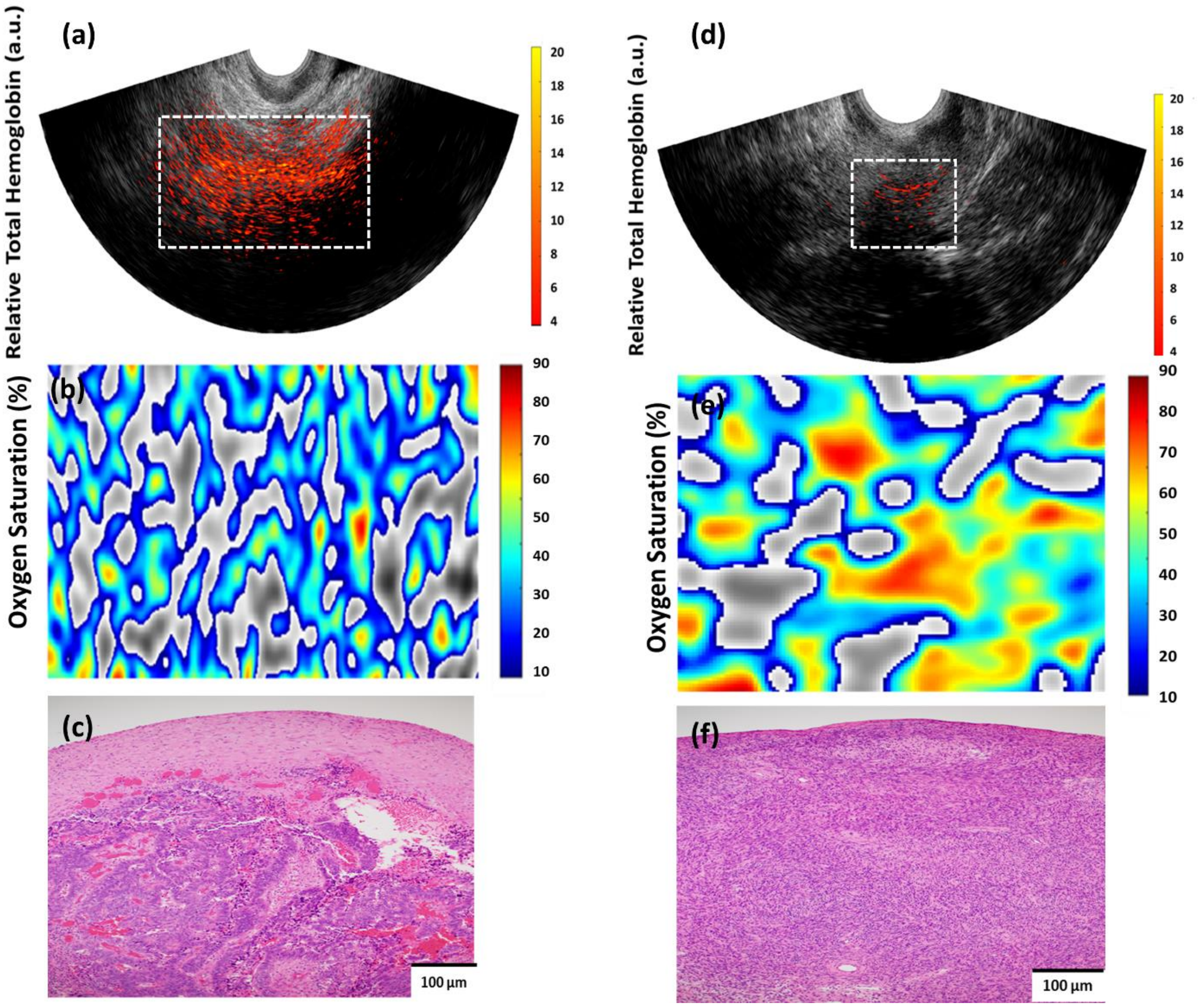

Figure. 5.1 PAT/US *in vivo* ovary study examples. PAT/US image, oxygen saturation and H&E images of the same patient for right ovary (a-c) and left ovary (d-f).

The results indicate that co-registered PAT/US imaging was able to successfully identify the extensive vasculature and angiogenesis in epithelial tumors as compared with the benign/normal ovaries, while the oxygen saturation was distinguishable between both the epithelial as well as other tumor types from the benign/normal ovary group. The differences of the functional photoacoustic features (rHbT and sO_2) were found to be highly significant compared to the conventional CA-125, which is limited to a single value for each patient and cannot distinguish between the ovaries of the same patient.

5.4 Summary

In summary, the feasibility of using co-registered PAT/US imaging for *in vivo* diagnosis of ovarian cancer was studied. The initial clinical results indicate that the epithelial ovarian cancers have much higher tumor vasculature as well as lower oxygen saturation, as compared to the benign/normal ovaries. The results from the imaging study was confirmed by histopathology diagnosis. This shows the potential of PAT/US imaging as a functional tool for in accurate *in vivo* diagnosis and assessment of human ovarian cancer.

References

[1] U.S. Preventive Services Task Force. "Screening for Ovarian Cancer: Recommendation Statement," (2004).

[2] Nossov V., Amneus M., Su F., Lang J., Janco J.M., Reddy S.T. and Farias-Eisner R., "The early detection of ovarian cancer: from traditional methods to proteomics. Can we really do better than serum CA-125?" Am J. Obstet. Gynecol. 199(3), 215-223 (2008).

[3] Tammela J. and Lele S., "New modalities in detection of recurrent ovarian cancer," Curr. Opin. Obstet. Gynecol. 16(1), 5-9 (2004).

[4] Wang L. V. and Hu S., "Photoacoustic tomography: in vivo imaging from organelles to organs," Science 335, 1458-1462 (2012).

[5] Wang Y. et al, "In vivo integrated photoacoustic and confocal microscopy of hemoglobin oxygen saturation and oxygen partial pressure," Opt. Lett. 36, 1029-1031 (2011)

[6] Heijblom M. et al., “Photoacoustic Image Patterns of Breast Carcinoma and Comparisons with Magnetic Resonance Imaging and Vascular Stained Histopathology.” Scientific Reports 5:11778 (2015).

[7] Dogra V. S. et al. “Multispectral Photoacoustic Imaging of Prostate Cancer: Preliminary Ex-Vivo Results.” Journal of Clinical Imaging Science 3:41 (2013).

[8] Attia A. B. E. et al. “Noninvasive Real-Time Characterization of Non-Melanoma Skin Cancers with Handheld Optoacoustic Probes.” Photoacoustics 7:20–26 (2017).

[9] Yang M. et al. “Photoacoustic/ultrasound Dual Imaging of Human Thyroid Cancers: An Initial Clinical Study.” Biomed. Opt. Express 8 (7) (2017).

[11] Salehi HS, Li H, Merkulov A, et al, “Coregistered photoacoustic and ultrasound imaging and classification of ovarian cancer: ex vivo and in vivo studies,” J. Biomed. Opt., 21(4), (2016).

Chapter 6 Conclusion and Future Work

In this dissertation, optical and photoacoustic imaging modalities were applied for *ex vivo* and *in vivo* diagnosis and assessment of human ovarian and colorectal cancer. Quantitative optical properties related to tissue absorption, scattering as well as morphological heterogeneities were evaluated and classified for discriminating benign/normal and malignant tissues.

In the first study, the feasibility of a phase stabilized swept source OCTE system was shown for estimating the strain inside human ovarian tissue and measure the correlation between the measured strain with the ovarian tissue collagen content. The collagen content inside the tissue was quantified by Sirius Red staining and found to have a strong negative correlation with the average strain. The initial results indicate that OCTE can be a powerful tool for measuring the micro-mechanical neoplastic changes associated with ovarian cancer.

In the second study, we imaged and classified human ovarian tissue using full field optical coherence tomography (FFOCT) system. We extracted quantitative features from the normal and malignant ovarian tissue images related to the morphological heterogeneity.

In the third study, we have developed an SFDI system to characterize *ex vivo* human ovarian and colon tissue samples and extracted several spatial and spectral features. Highly significant difference was observed between the absorption, scattering, HbT, scatter slope as well as spatial heterogeneities of the normal and malignant ovary and colon tissue groups. Work is going on to develop a next generation miniaturized portable LED based SFDI system that can be readily used as a guiding tool for intraoperative image guided surgery.

In the final study, high-risk patients were imaged *in vivo* with co-registered photoacoustic tomography and ultrasound (PAT/US) system to detect angiogenetic and hypoxic changes associated with development and progression of ovarian cancer. Significant differences were observed between the epithelial and other tumor types with benign/normal ovaries in terms of blood hemoglobin and oxygenation. We are currently acquiring more data from patients at the Washington University School of Medicine. We hope to provide the physicians with an *in vivo* functional imaging tool for early detection and accurate diagnosis of ovarian cancer. Currently, work is going on to apply PAT/US imaging for diagnosis of human colorectal cancer.

Vita

Sreyankar Nandy

EDUCATION

2018 (expected)	**Washington University in St. louis** Ph.D. in Biomedical Engineering
2013	**Indian Institute of Technology, New Delhi, India.** M.Tech. in Applied Optics
2010	**Indian Institute of Engineering Science and Technology, Shibpur, India.** M.Sc. in Applied Physics
2007	**University of Calcutta, Kolkata, India.** B.Sc. (Hons.) in Physics

PEER REVIEWED JOURNAL PUBLICATIONS

1. **Sreyankar Nandy***, Atahar Mostafa*, Ian Hagemann, Matthew Powell, Eghbal Amidi, David Mutch, Catherine Robinson, Cary Siegel and Quing Zhu, "Role of Co-Registered Photoacoustic and Ultrasound Tomography: Initial Application for Evaluation of Ovarian Cancer", Radiology, *in press* (2018).

2. **Sreyankar Nandy***, William Chapman Jr.*, Rehan Rais, Ivan Gonzalez, Deyali Chatterjee, Matthew Mutch and Quing Zhu, "Label-free quantitative optical assessment of human colon tissue using spatial frequency domain imaging", Techniques in Coloproctology, *in press* (2018).

3. **Sreyankar Nandy,** Ian S. Hagemann, Matthew A. Powell, David Mutch, Cary Siegel, Quing Zhu, "Quantitative Multispectral Optical Evaluation of Human Ovarian Tissue Using Spatial Frequency Domain Imaging," Biomed. Opt. Express 9(5), 2451-2456 (2018).

4. **Sreyankar Nandy**, Melinda Sanders, and Quing Zhu, "Classification and analysis of human ovarian tissue using full field optical coherence tomography," Biomed. Opt. Express 7 (12), 5182-5187 (2016).

5. **Sreyankar Nandy**, Atahar Mostafa, Patrick Kumavor, Melinda Sanders, Molly Brewer and Quing Zhu, "Characterizing optical properties and spatial heterogeneity of human ovarian tissue using spatial frequency domain imaging", Journal of Biomedical Optics 21 (10), 101402-101402 (2016).

6. **Sreyankar Nandy**, Hassan S. Salehi, Tianheng Wang, Xiaohong Wang, Melinda Sanders, Angela Kueck, Molly Brewer, and Quing Zhu, "Correlating optical coherence elastography based strain measurements with collagen content of the human ovarian tissue," Biomed. Opt. Express 6 (10), 3806-3811 (2015).

7. Tianheng Wang, **Sreyankar Nandy**, Hassan S. Salehi, Patrick D. Kumavor, and Quing Zhu, "A low-cost photoacoustic microscopy system with a laser diode excitation," Biomed. Opt. Express 5 (9), 3053-3058 (2014).

8. Vishal Srivastava, **Sreyankar Nandy**, Dalip Singh Mehta, “High-resolution full-field spatial coherence gated optical tomography using monochromatic light source,” Applied Physics Letters 103, 103702 (2013).

9. Vishal Srivastava, Sreyankar Nandy, Dalip Singh Mehta, “High-resolution corneal topography and tomography of fish eye using wide-field white light interference microscopy,” Applied Physics Letters 102, 153701 (2013).

10. Yifeng Zheng, Bin Rao, **Sreyankar Nandy**, William Chapman Jr., and Quing Zhu, “The Angular Spectrum of the Scattering Coefficient Map Reveals Subsurface Colorectal Cancer,” *under review*.

11. Mohsen Erfazandeh, **Sreyankar Nandy**, Patrick D. Kumavor and Quing Zhu, “A low-cost handheld multispectral spatial frequency domain imaging prototype for tissue characterization,” *under review.*

12. Xiandong leng, William Chapman Jr., Bin Rao , **Sreyankar Nandy**, Ruimin Chen, Rehan Rais, Ivan Gonzalez, Qifa Zhou, Matthew Mutch and Quing Zhu, “Feasibility of co-registered Ultrasound and Acoustic-resolution photoacoustic imaging of human colorectal cancer,” *under review.*

13. Guang Yang, Eghbal Amidi, **Sreyankar Nandy** and Quing Zhu, “Optimized light delivery design using ball lens for co-registered photoacoustic and ultrasound endo-cavity imaging,” *in preparation.*

14. Yifeng Zeng, **Sreyankar Nandy,** Ian Hagemann, Bin Rao, Yixiao Lin, Lindsay Kuroki, Andrea Hagemann, David Mutch, Matthew Powell, Quing Zhu, “Quantitative 3-dimensional depth resolved scattering features for identification of human ovarian cancer using optical coherence tomography,” *in preparation*.